Title: A Multi Mega Watt Continuous Wave RF Window for Particle Accelerator Applications

Final Technical Report for the SBIR Phase I

Grant # DE-FG02-02ER83561

DOE Patent Clearance Granted 3/3/04
Date

Daniel O. Park
(630) 252-2308
E-mail daniel.park@ch.doe.gov
Office of Intellectual Property Law
DOE Chicago Operations Office

DISCLAIMER

DISCLAIMER

Portions of this document may be illegible in electronic image products. Images are produced from the best available original document.

Technical Results From the Phase I Work 2
Summary 2
Thermal Stress Analysis 2
MP Analysis 6
Objective 6
Summary of results 6
Model 7
Results 8
MP at a higher SEY for the ceramic surface 13
Conclusion 14

Technical Results From the Phase I Work

Summary

In the phase I project all tasks of the work plan have been completed. Stress analysis have been performed for three separate window geometries yielding overall stress distribution at the 10 Megawatt power level. The thin cylindrical shell having a characteristic impedance of 10 ohms with ¼ wave matching sections on either side demonstrated the lowest stress levels at full power. The maximum tensile stress in this geometry using TPA window material is 0.1E*8 Pa. Multipacting analysis was completed and no significant multipacting appeared at any power level up to 10 Mega Watts using a pessimistic SEY of 2.5 for the ceramic coating. A comparison of candidate materials with regard to all relevant electrical and thermal mechanical properties identified Translucent Polycrystalline Alumina (TPA) as a preferred choice. A complete set of engineering drawings along with a production plan was produced for the window assembly.

Thermal Stress Analysis

Case #/Title	Outer Diameter (cm)	Inner Diameter (cm)	Thickness (cm)	Impedance (Ω)	Temp. Difference (K)	Radial Tensile Stress Sx (Pa)	Axial Tensile Stress Sy (Pa)	Azimuthal Tensile Stress Sz (Pa)
#1 –Thick Annulus	9.53 (3.75")	5.72 (2.25")	10.0 (3.937")	9.7	24.2	.342E+08	.593E+08	.551E+08
#2 – Thin Annulus	9.53 (3.75")	8.89 (3.5")	10.0 (3.937")	1.3	3.2	.478E+07	.734E+07	.712E+07
#3 –Planar Window	9.53 (3.75")	2.54 (1.0")	2.5 (0.984")	20.8	62.2	.537E+08	.115E+09	.131E+09

Table 1. Thermal and Structural Results for Three Unrestrained Window Geometries.

A window that provides both acceptable RF matching and minimized thermally induced stresses is the most desirable. For initial studies, three basic shapes were investigated – a thick annulus, a thin annulus and a planar window. It should be noted that the impedance varies greatly for the three geometries chosen. For each case, the inner and outer surface temperatures were fixed and the exterior surface of the ceramic was unrestrained. The reference temperature used for calculating thermal strain was 293 K. The loss tangent for 95% Alumina was used for all cases. The internal heat generation was calculated for each volume as described in the Phase I Proposal Appendix A and input into each of the models. Typical total power depositions in the ceramic volume were approximately 7 kW for 10 MW of transmitted power.

Material Property	95% Alumina	Alumina Nitride	TPA
Modulus of Elasticity (GPa)	370	300	400
Tensile Yield Strength (Pa)	1.72E+08	2.96E+08	0.8E+08
Poisson's Ratio	0.22	0.22	0.22
Thermal Conductivity (W/m-K)	29.4	115	30
Dielectric Constant	10	8.5	10.1
Loss Tangent	0.00014	0.003	0.0000245
Thermal Expansion (m/m-K)	6.9E-6	5.7E-6	5.4E-6

Table 2. Candidate materials for High Power Window Assembly

The average body temperature and the overall temperature difference in the body are the two factors which directly affect the magnitude of the thermal stresses. The highest temperature difference was found in the planar window case where the thermal path to the temperature sink is the longest. The lowest temperature difference was found in the thin annulus, which possessed the shortest radial thermal path. The planar window (Case #3) stresses exceeded the tensile strength of the window material, and therefore was deemed an unacceptable geometry. Calculated stresses for both the thick and thin annular window geometries were below the tensile yield strength of the 95% alumina. Of the two viable designs, the thick window (Case #1) with an impedance of 9.7 Ω, was more desirable when considering RF matching of the window assembly into a waveguide system.

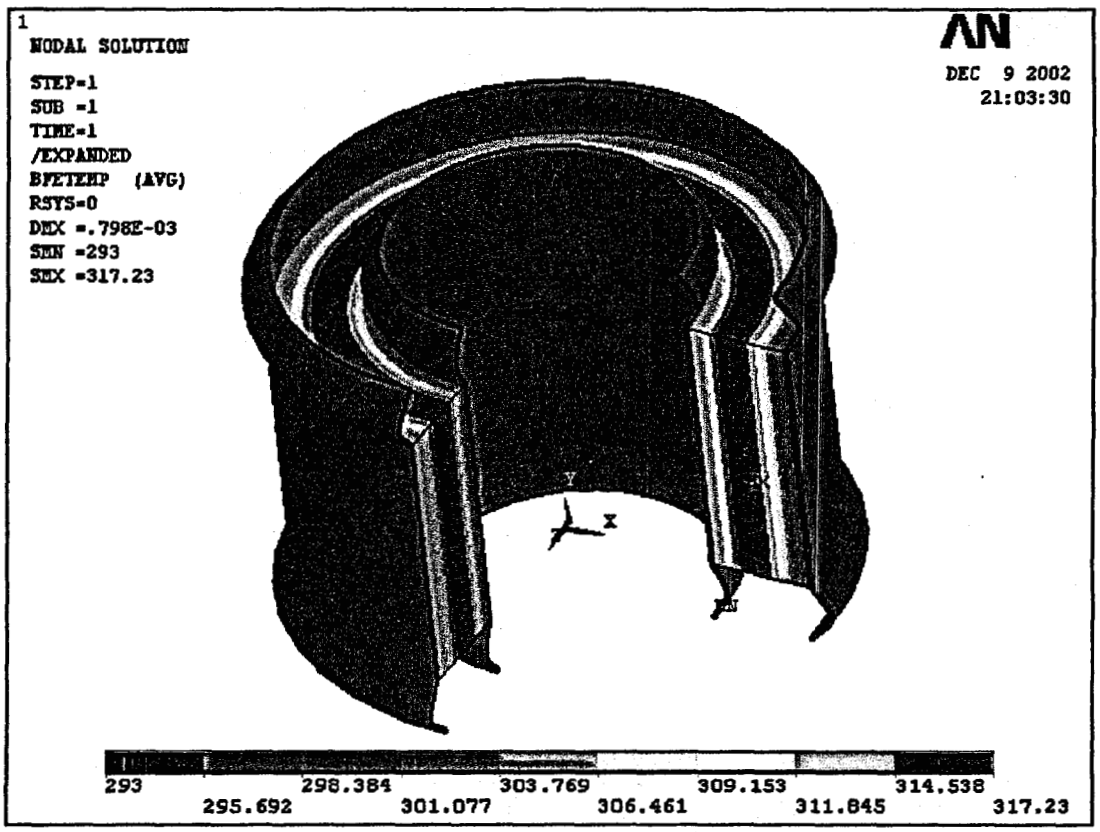

Figure 3. Cut-away View of the Window: Peak temperature for 95% Alumina is 24 K higher than inner and outer water-cooled surfaces.

Next, in order to closely approximate the unrestrained boundary condition, thin copper tubes were added to the thick annulus solid model. The temperatures on the inner and outer surfaces of the copper tubes were fixed at 293 K. The ends of the tubes, 25 mm beyond the window ends, were fully restrained. The volumetric power deposition was applied in the same manner as in the initial studies. The three different materials listed in Table 3. were investigated – 95% Alumina, Alumina Nitride and Translucent Polycrystalline Alumina (TPA). The TPA had the lowest loss tangent and therefore exhibited the lowest temperatures and associated stresses (Table X). The 95% Alumina temperatures and stresses were higher but well within acceptable limits. The Alumina Nitride temperatures were the highest and as a result the stresses exceeded the tensile yield strength of the material.

Material	Temp. Difference (K)	Radial Tensile Stress Sx (Pa)	Axial Tensile Stress Sy (Pa)	Azimuthal Tensile Stress Sz (Pa)
95% Alumina	24.2	.348E+08	.629E+08	.554E+08
Alumina Nitride	125.2	.115E+09	.212E+09	.183E+09
TPA	4.2	.884E+07	.925E+07	.102E+08

Table 3. Comparison of Temperature Differential and Peak Tensile Stresses for a window with outer radius = 9.53 cm, inner radius = 5.72 cm, thickness = 10 cm and impedance = 9.7 Ω

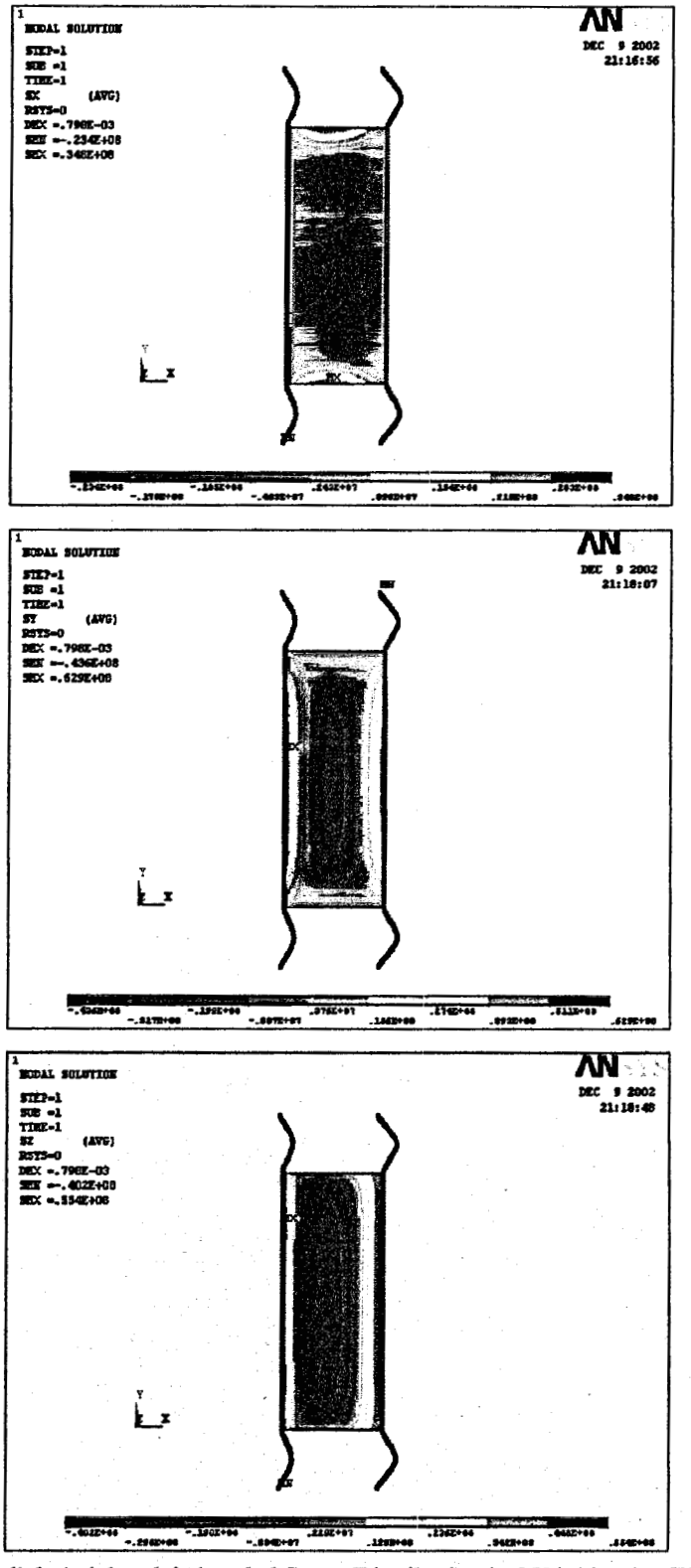

Figure 4a, 4b, and 4c. Radial, Axial and Azimuthal Stress Distribution in 95% Alumina Window with Thin Copper Tubes to Provide Strain Relief

The copper tubes used for strain relief function well at near room temperatures. However, the window assemblies will be brazed at over 1000°C in a vacuum furnace. As a result, the copper will become fully annealed. An alternative copper-based material is proposed for the High Power Window assemblies. This material, GlidCop®, is an alumina-dispersion-strengthened alloy with nearly the same thermal and electrical properties of copper. In addition, the material retains its strength after annealing. As more alumina is added to the copper matrix, the strength increases but the thermal and electrical properties decrease as compared with OFE copper. GlidCop® AL-15 is chosen as a substitute for the thin OFE copper tubes. It is expected that the 10% reduction in thermal conductivity will not appreciably affect the temperatures and stresses within the ceramic window.

Material Property	OFE Copper	GlidCop® AL-15
Modulus of Elasticity (GPa)	128	128
Poisson's Ratio	0.36	0.36
Thermal Conductivity (W/m-K)	398	365
Thermal Expansion (m/m-K)	16.8E-6	16.8E-6
Fully Annealed Yield Strength (Pa)	0.41E+08	2.55E+08

Table 4 Comparison of Material Properties for Copper and GlidCop®

	GLIDCOP® AL-15	GLIDCOP® AL-25	GLIDCOP® AL-60
Al_2O_3	.3 wt%	.5 wt%	1.1 wt%
Cu	Balance	Balance	Balance
Electrical Conductivity	54 Meg S/m 92% IACS	50 meg S/m 87% IACS	45 meg S/m 78% IACS
Thermal Conductivity (W/m-K)	365	344	322
Yield Strength (with 0% cold work) (MPa)	255-331	296-372	413-517
Yield Strength (with 70% cold work) (MPa)	441-517	469-544	551-600
Yield Strength (after 1000° anneal) (MPa)	255-331	296-372	413-517

Table 5 Comparison of Material Properties for three varieties of GlidCop®

MP Analysis

Objective

Evaluate the multipacting (MP) characteristics of a 750MHz 10MW window design.

Summary of results

No MP barrier is found on the vacuum side ceramic surface up to 10MW forward power for all the three load conditions considered, namely a matched load (traveling wave), a shorted load (full reflection), and an open load (full reflection). Two mild MP barriers are identified at 7-8MW (traveling wave) on the metal surface of the matching section OC of the vacuum side. All possible phases of the standing wave pattern in full reflection were not examined but are left to full power testing. The multipacting analysis can identify early design problems while it is unable to provide

certainty in design success and testing of window designs is the only certain measure of freedom from multipacting.

Model

The window design has been optimized from RF point of view. The dielectric constant of the ceramic material is 10. The ceramic window has dimension of 2.25" (5.72cm) IR, 3.75" (9.53cm) OR, 3.937" (10cm) length. Two matching sections are symmetric about the ceramic and each has dimension of 2.25" (5.72cm) IR, 3.75" (9.53cm) OR, 3.52" (8.94cm) length. Beyond the matching sections are two coaxial sections, each has dimension of 0.787" (2cm) IR, 3.75" (9.53cm) OR, 3.937" (10cm) length. Fig. 1 is a graphical description of the model.

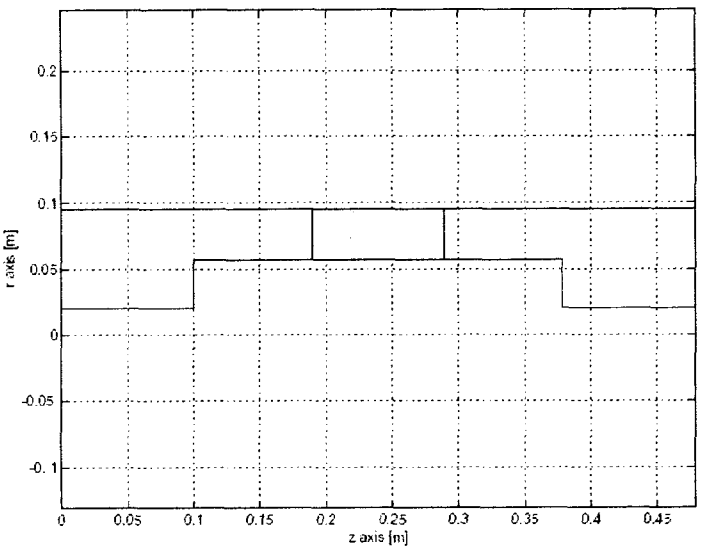

Figure 1 Model of the 750MHz 10MW window for MP calculations.

The left side of the window assembly will be called the air side and the right side the vacuum side. To facilitate the MP code, sometimes the coax line of the vacuum side is extended by 10cm (a quarter wavelength).

Secondary electron yield (SEY): For the base line simulation runs, it is assume that the SEY of the Ti/N coated ceramic surface is the same as that of the metal surface of the conductors. The maximum SEY is 1.5 at a 400eV of impact energy. For some exploration runs, the SEY of the ceramic surface is raised by a factor of 2.5/1.5 so as that the maximum SEY is 2.5 at a 400eV. Both SEY curves are shown in Fig. 2.

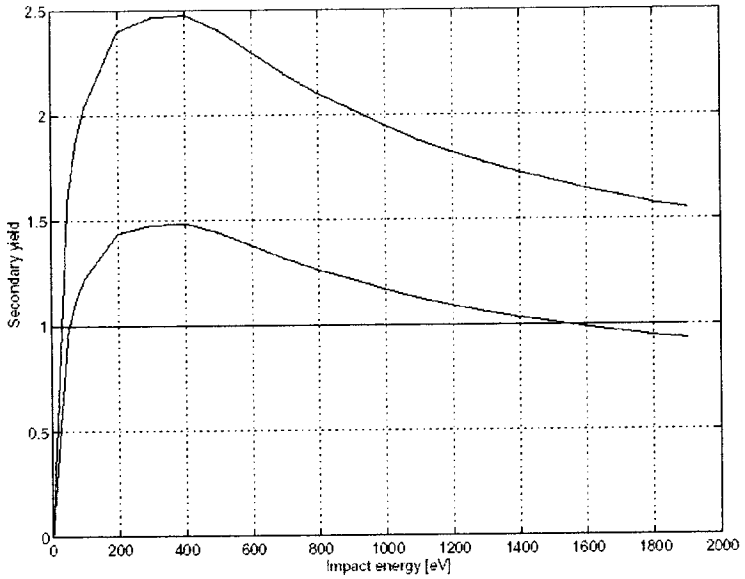

Figure 2 Secondary electron emission yield used for the ceramic surface.

Results

Traveling wave

In the traveling wave mode, MP barriers are searched for at a 25kW (0.25% of 10MW) power step. Initial search was focused on the ceramic surfaces only. Later the search was extended to include the metal surfaces of the matching section of the vacuum side. Fig. 3 shows the results.

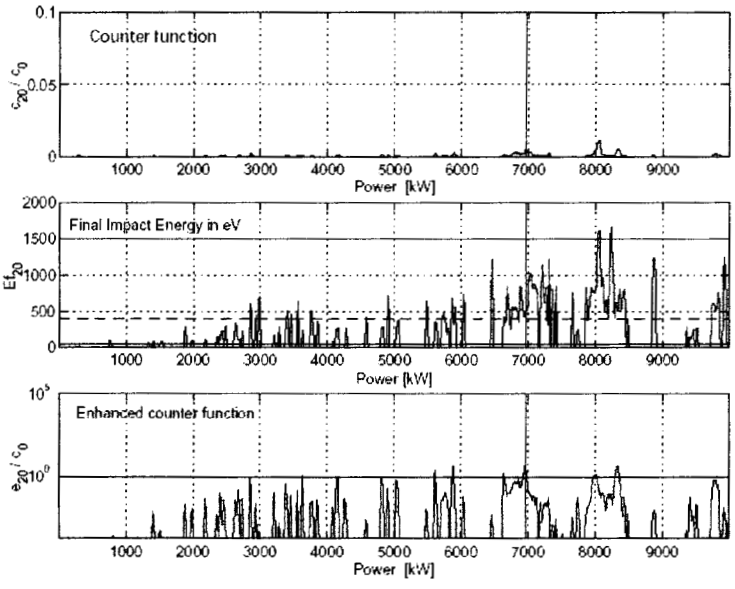

Figure 3 MP characteristics of the vacuum side of the window assembly.

The bottom graph shows that there are two MP barriers in the neighborhood of 7MW and 8MW. These two barriers are likely to be very "soft" as indicated by an enhanced counter function on the order of ~1. The middle graph shows the corresponding impact energy. Trajectory calculations reveal that these multipactors occur on the OC of the matching section near the ceramic surface (see Fig. 4). Note that the ceramic surface does not participate in these MP's.

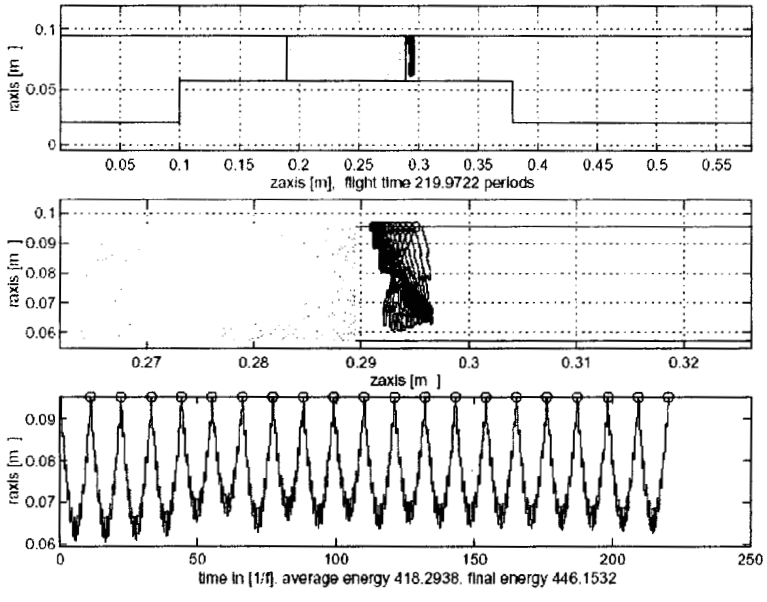

Figure 4 Electron trajectory of MP bands (7MW and 8MW) on the vacuum side of the window assembly.

Similar MP search was performed for the air side of the window. Near 4MW, a two-sided MP was identified for which both the ceramic surface and the metal surface of the OC of the matching section are involved (see Fig. 5 for the trajectory). This MP has a much higher degree of "hardness", indicated by a large enhanced counter function as shown in Fig. 6. In practical applications, the air side of this window will be at 1 atmospheric pressure. For this reason, the above-described MP will actually not be able to develop – even though such a process is possible from solely kinematic point of view.

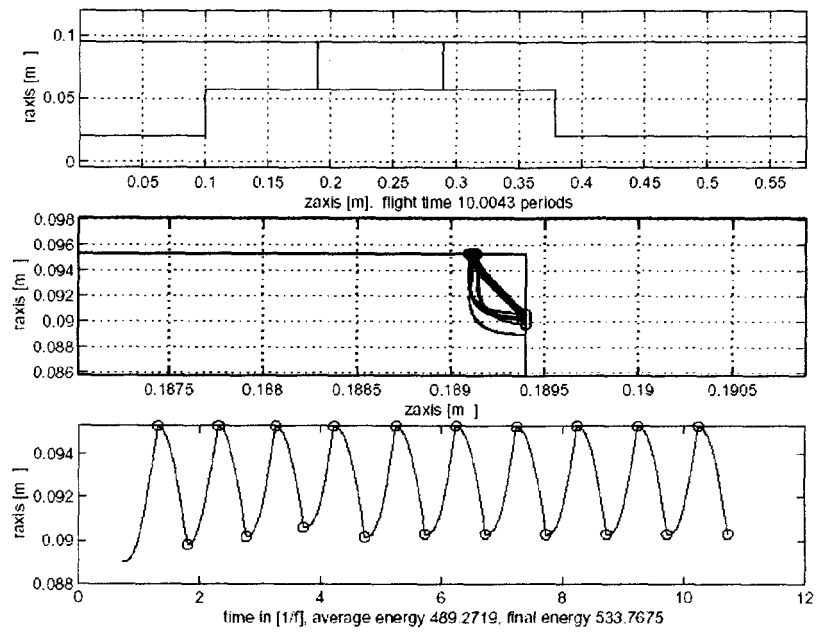

Figure 5 Two-sided MP at 4MW on the air side (if under vacuum).

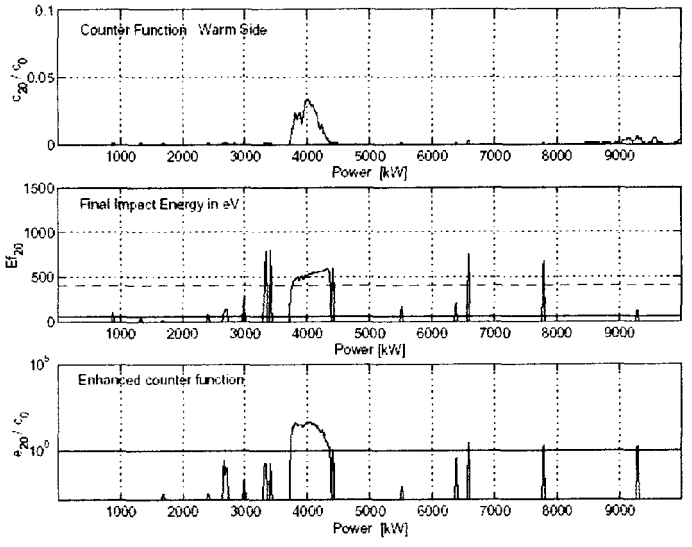

Figure 6 MP characteristics of the air side (if under vacuum) for the traveling wave mode.

Full reflection

The extended model (The coax line on the vacuum side was extended by 10cm) was used for the full reflection case (to minimize the load effect on the accuracy of the field solution in the window region). Two load conditions were considered, open and short. For an open load, no MP was found on either side of the window. For a short load, no MP was found on the vacuum side either. But a one-sided MP was identified on the ceramic surface of the air side. The characteristics and electron trajectory of this MP is shown in Fig. 7 and 8 respectively.

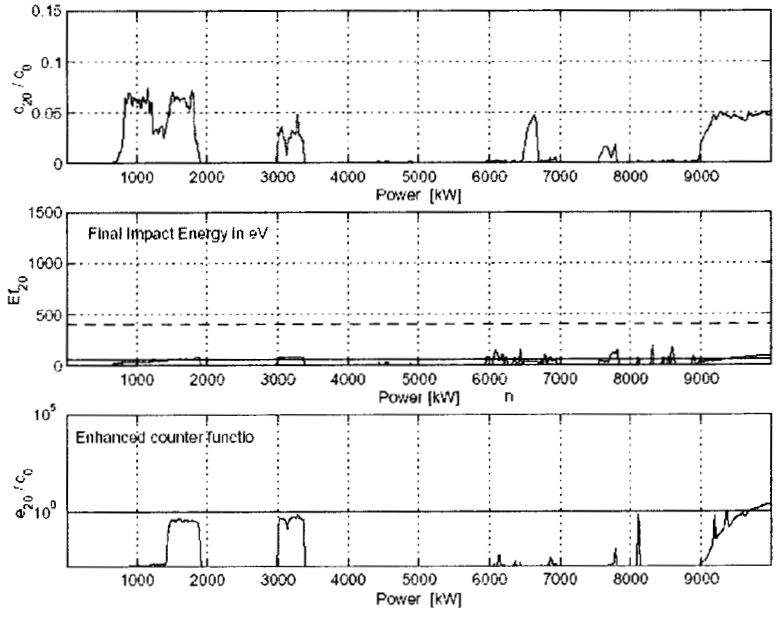

Figure 7 MP characteritics of the air side (if under vacuum) of the extended model with a short load.

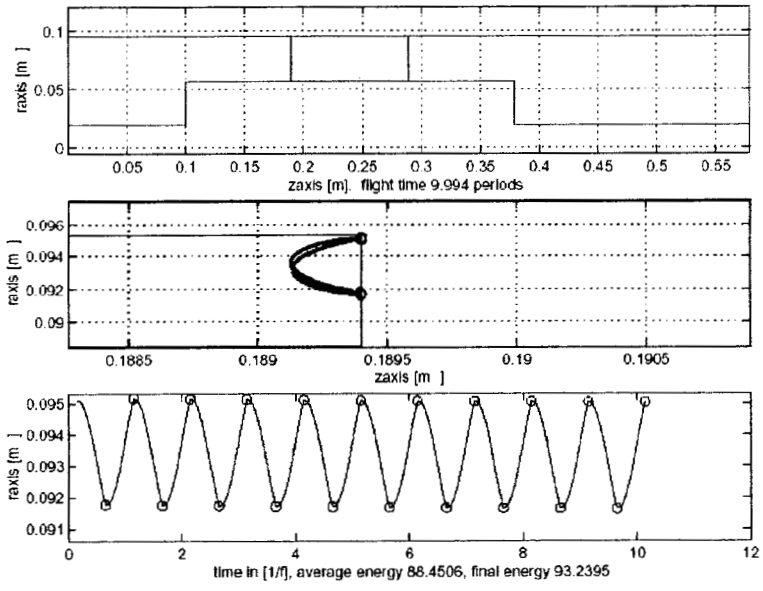

Figure 8 Electron trajectory of the MP bands of the air side (if under vacuum) of the extended model with a short load.

MP at a higher SEY for the ceramic surface

Since the SEY of a Ti/N coated ceramic surface is not a well-controlled parameter in real situations, it is necessary to repeat the calculations using a more pessimistic number. For this purpose, the base line SEY curve is scaled upward by a factor of 2.5/1.5. The resultant SEY curve has a similar shape but the maximum SEY is now 2.5 at 400eV (see Fig. 2).

Fig. 9 and 10 shows the MP characteristics of the vacuum and air side respectively for the traveling wave case with an alleviated SEY.

Comparing Fig. 9 with Fig. 3, it is seen that the MP characteristics of the vacuum side in the traveling wave mode remain the same for a higher SEY value of the ceramic surface. This observation becomes apparent when one realizes that the two MP barriers near 7MW and 8MW involve only the OC of the matching section as shown in Fig. 4. The fact that no new MP barrier shows up at a higher SEY for the ceramic surface suggests that no MP barrier has been overlooked with the base line SEY. The conclusion is then (at a higher level of confidence) that the ceramic surface does not participate in the MP's on the vacuum side in the traveling wave mode.

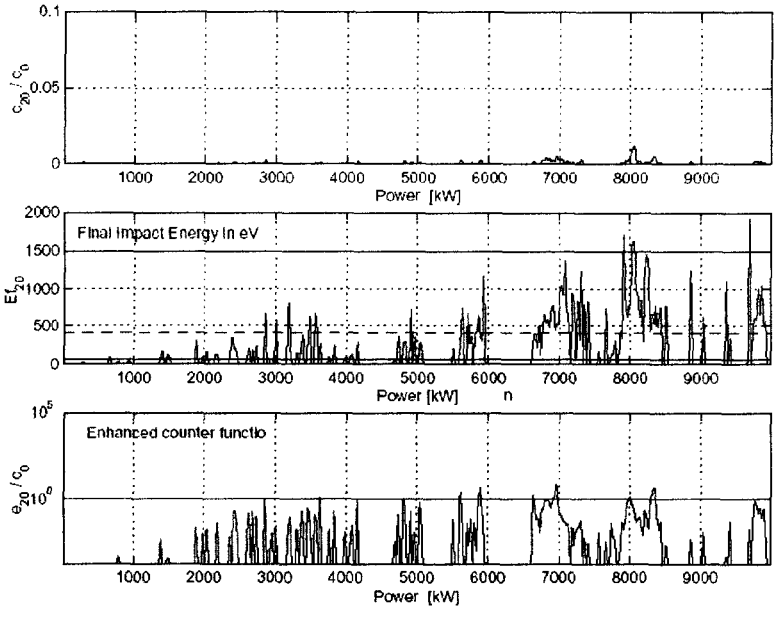

Figure 9 MP chraracteristics of the vacuum side in the traveling wave mode. Maximum SEY is 2.5 at 400eV.

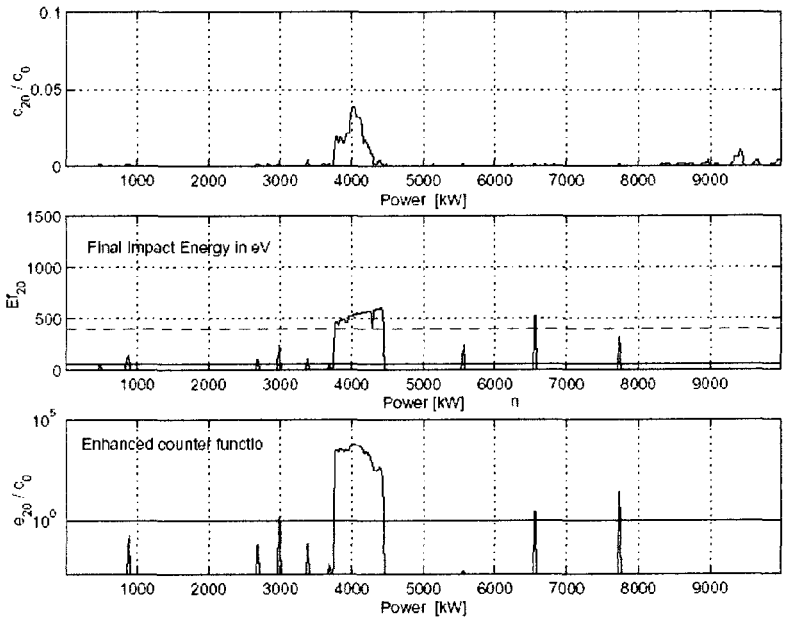

Figure 10 MP characteritics of the air side (if under vacuum) in the traveling wave mode. Maximum SEY is 2.5 at 400eV.

Comparing Fig. 10 with Fig. 6, it is seen that the MP on the air side is intensified when the higher SEY is used for the ceramic surface – as it should be because this MP involves the ceramic surface as shown in Fig. 5.

Repeated calculations for the full reflection case with an alleviated SEY rendered similar effect as for the traveling wave case. No MP barrier on either side was observed when the extended model has an open load. With a shorted load, no MP barrier was found at the vacuum side; one-sided MP, at an intensified level, was found at the air side (if under vacuum).

Conclusion

In this analysis the proposed 10MW window design is free of multipacting on the ceramic surface for the full power range, both in the traveling wave and full reflection mode. Near 7MW and 8MW in the traveling wave mode, multipacting might show up on the outer conductor of the matching section. These multipacting barriers are however very soft and are expected to be easily eliminated by regular RF processing. As mentioned earlier the multipacting analysis can identify early design problems while it is unable to provide certainty in design success and testing of window designs is the only certain measure of freedom from multipacting.